Electronic Supplementary Material (ESI) for ChemComm.

Supplementary Information

Bulk-immiscible CuAg alloy nanorods prepared by phase transition from oxide for electrochemical CO_2 reduction

Yihong Yu[1], Di Wang[1], Yimeng Hong[1], Teng Zhang[1], Chuangwei Liu[1], Jing Chen[2], Gaowu Qin[1], Song Li[1,3,*]

[1] Key Lab for Anisotropy and Texture of Materials (MoE), School of Materials Science and Engineering, Northeastern University, Shenyang 110819, China

[2] College of Electronics and Information Engineering, Shenzhen University, Shenzhen 518060, China

[3] Institute for Frontier Technologies of Low-Carbon Steelmaking, Liaoning Province Engineering Research Center for Technologies of Low-Carbon Steelmaking, Northeastern University, Shenyang 110819, China

* E-mail: lis@atm.neu.edu.cn

Materials and methods

Sample preparation.

Sodium hydroxide (NaOH, ≥ 99.0%), potassium hydroxide (KOH, ≥ 99.0%), silver nitrate ($AgNO_3$, ≥ 99.0%), copper nitrate trihydrate ($Cu(NO_3)_2 \cdot 3H_2O$, Mw = 241.60) Nafion perfluorinated resin solution (5 wt%), isopropyl alcohol (C_3H_8O, ≥ 99.7%), and ethanol (C_2H_6O, ≥ 99.7%) were purchased from Shanghai Aladdin Bio-Chem Technology Co., Ltd. All chemicals were used without further purification. The water used in all the experiments was purified through a microporous system (> 18.0 MΩ).

The CuAg alloy nanorods were synthesized as follows. Firstly, 3.87 g $Cu(NO_3)_2$ and 2.72 g $AgNO_3$ were dissolved in 10 mL H_2O. 20 mL of sodium hydroxide solution containing 2.43 g NaOH was added into above solution. After complete mixture, 20- and 40-ml extra water was added under stirring for 2 h for each stage. Constant Ar was introduced to prevent the formation of carbonate. The product was collected by centrifugation at 8000 rpm and repeatedly washed with water and ethanol. Finally, the solid was collected and dried at 70℃ for 24 h to obtain the $Cu_2Ag_2O_3$ nanorods. We used the following typical procedure to prepare the working electrode. 1 mg $Cu_2Ag_2O_3$ was dispersed in 950 μL Isopropyl alcohol and 50 μL 0.5 wt% Nafion solution, sonicating for 0.5 h to form a homogeneous ink. The mixture was then sprayed onto a 1 cm × 1 cm gas diffusion layer (GDL) and dried under an infrared lamp as an $Cu_2Ag_2O_3$ working electrode, and the actual loading of the $Cu_2Ag_2O_3$ catalyst was 1mg cm^{-2}. Then, the working electrode was electrochemically reduced in 1 M KOH electrolyte by applying a 5.0 V voltage for 3 s to produce the CuAg alloy nanorods.

For comparison, Cu and Ag nanoparticles were synthesized by using electroreduction of corresponding oxide nanoparticles in a similar way. 0.75 M silver nitrate was used as precursor solution. 0.32 g NaOH was added followed by 6 h of vigorously stirring. The product was collected by centrifugation and washed. Then, the solid of Ag_2O nanoparticles was collected and dried at 70℃ for 24 h. Finally, the Ag_2O nanoparticles was electrochemically reduced under a 5.0 V voltage for 3 s to obtain Ag nanoparticles (Ag-ER). Similarly, the Cu nanoparticles were obtained by electrochemical reduction from CuO (Cu-ER).

Materials characterizations.

X-ray diffraction (XRD) patterns were obtained from a Rigaku-D/max 2500 V instrument with a Cu Kα radiation source. The surface morphology and microstructure of the samples were observed by JSM-7001F scanning electron microscope (SEM). Transmission electron microscope (TEM) and aberration-corrected HAADF-STEM were probed by a FEI/Thermo scientific Themis Z microscope at acceleration voltage of 200 kV. X-ray photoelectron spectroscopy (XPS) profiles were performed on a Thermo Fisher 250Xi spectrometer with Al Kα X-ray radiation source.

XRD simulation

The four-atom unit cell of FCC was utilized to construct crystal structure of CuAg alloy. To reflect the solid-solution nature of CuAg alloy, the occupancy of Cu and Ag at each lattice site is set 0.5. The equilibrium lattice parameter of the CuAg model is relaxed to minimize the total energy by using first-principles calculation method in the framework of the exact muffin-tin orbit (EMTO)[1]. EMTO method is an improved Koringa-Kohn-Rostoker (KKR) approach that use the coherent potential approximation (CPA). A key advantage of the EMTO method is that it can be combined with CPA technique to simulate chemical disordered solid solutions. The relaxed lattice parameter is 0.395 nm. Next, the powder XRD profile based on the relaxed parameter is simulated by using the software package of VESTA[2].

Electrochemical measurements and product analysis

Electrochemical measurements in flow cell. CO_2RR measurements were performed on a flow cell with an electrochemical workstation. The flow cell consists of three independent chambers: a cathode, a gas, and an anode chamber. Anion exchange membranes (AEM) are used to separate the anode and cathode compartments. The Ag/AgCl reference electrode is placed in the cathode chamber through the top hole. A multicomponent $Mn_5Co_{10}Fe_{30}Ni_{55}O_x$ oxide optimized by high-throughput technique was used as electrocatalyst at counter electrode. Under the operation of the dual-channel

[1] Vitos L. Computational Quantum Mechanics for Materials Engineers[M], London: Spring, 2007.
[2] https://jp-minerals.org/vesta/en/

peristaltic pump, 1 M KOH solution is circulated to the anode and cathode chambers at a constant flow rate of 10 sccm (mL min^{-1}). A high-purity CO_2 gas stream of 20 sccm was supplied to the gas chamber controlled by a digital mass flow controller. The ohmic loss between the reference electrode and the working electrode was measured at 1 M KOH by electrochemical impedance spectroscopy and applied 85% ohmic resistance correction in all measurements. Linear sweep voltammetry (LSV) was performed at a sweep rate of 5 mV s^{-1}.

Product Analysis. The liquid products were detected by ^1H NMR (BRUKER AVANCEAV III HD 500). The NMR samples were prepared by mixing 0.5 mL of cathode electrolyte after CO_2RR with 800 μL of deuterated water (D_2O), and 0.4 μL of dimethyl sulfoxide (DMSO) was added as an internal standard. Pre-saturation method was used to suppress water peak.

The faradaic efficiency of liquid products was calculated with the equation:

$$FE_l(\%) = \frac{q_1}{Q} = \frac{Fc_1Vz_1}{Q} \times 100\%$$

Q: the total charge passed (C); q_1: the partial charge to produce species; F: 96485 C mol^{-1}; c_1: the concentration of species (mol L^{-1}); V: the electrolyte volume (L); z_1: the number of exchanged electrons to produce species.

During the chronoamperometric measurement, the gas products were directly introduced from the flow cell into the gas chromatograph (Agilent 7890A GC System), which was equipped with TDX-01 and HP-AL/KCL columns for quantifications. The gas products were analyzed by gas chromatography. CO and H_2 in the gas products were analyzed by a thermal conductivity detector (TCD), and the flame ionization detector (FID) was used to analyze the hydrocarbons in the gas products with Ar as the carrier gas.

The faradaic efficiency of gas products was calculated with the equation:

$$FE_g(\%) = V_i v \frac{nFp_0}{RT_0 i}$$

V_i: the volume concentration of gas products based on a calibration of the GC; v: flow rate; n: number of transferred electrons for the certain product; F: 96485 C mol^{-1}; T_0: the temperature for testing; i: the current measured during a constant-potential electrolysis. p_0: 1.013 bar; R: 8.314.

The formation rate for products was calculated with the equation:

$$R = (q_{tot} \times FE)/(96485 \times n \times t \times S)$$

q_{tot}: the total charge; t: the electrolysis time (h); S: the geometric area of the electrode (1 cm^2).

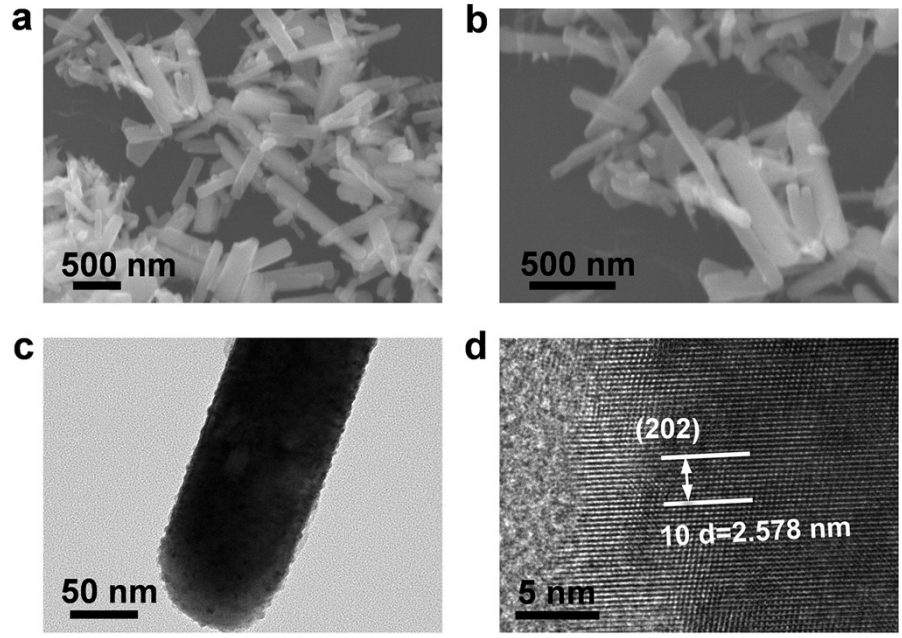

Figure S1. Characterization of $Cu_2Ag_2O_3$ precursor for electro-reduction synthesis of CuAg solid-solution alloy. (a, b) SEM morphology of $Cu_2Ag_2O_3$ nanorods. (c) TEM image showing nanorod shape of $Cu_2Ag_2O_3$. (d) HRTEM image of $Cu_2Ag_2O_3$ showing the lattice fringe of (202) plane.

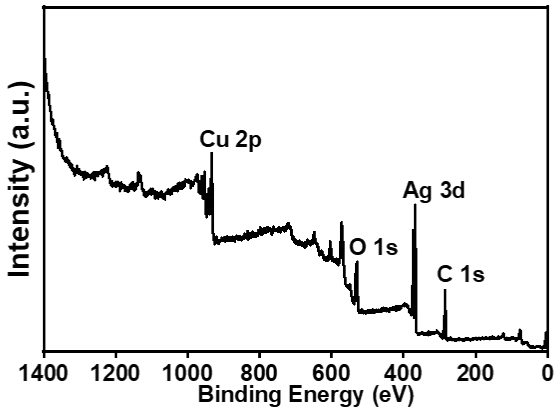

Figure S2. XPS survey spectrum of $Cu_2Ag_2O_3$ nanorods, indicating the presence of Cu, Ag, and O.

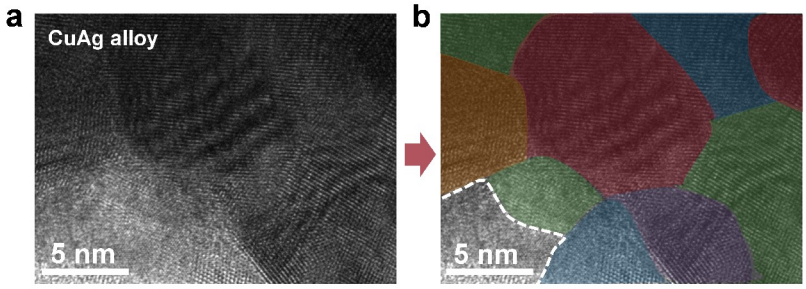

Figure S3. (a-b) TEM images showing the polycrystalline nature of the reduced CuAg nanorod. The image in (b) is colored according to crystal orientation to distinguish separate crystals.

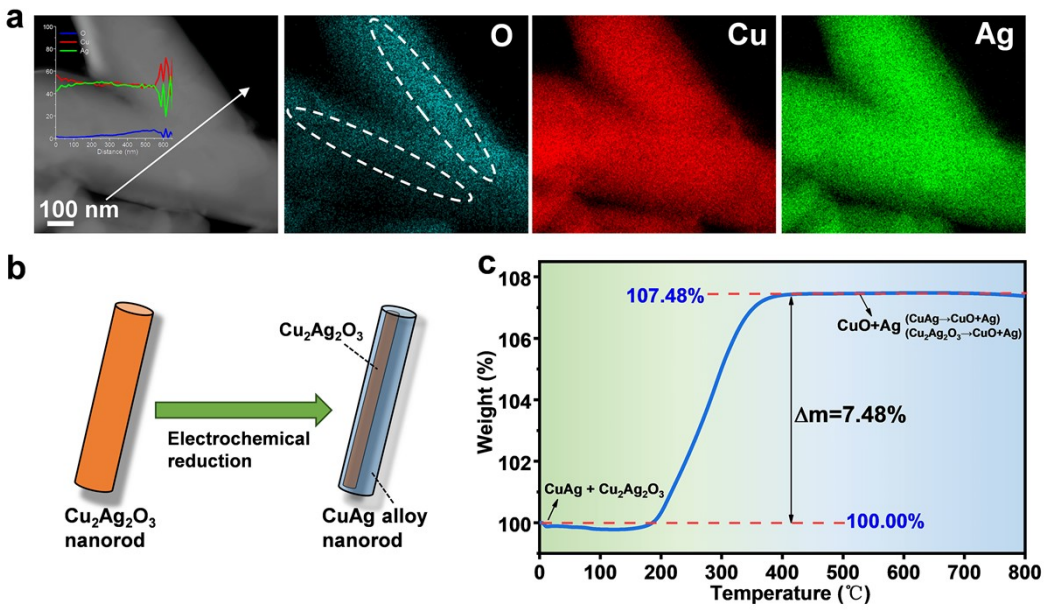

Figure S4. (a) STEM-EDS mapping of nanorods after electroreduction, showing that oxygen is resident in the core. Element line scan analysis diagram is inserted in the inset. (b) Schematic diagram of phase transition of $Cu_2Ag_2O_3$ to CuAg alloy by electro-reduction under large overpotential. (c) Thermogravimetric (TG) curve of electro-reduced nanorods in oxygen atmosphere.

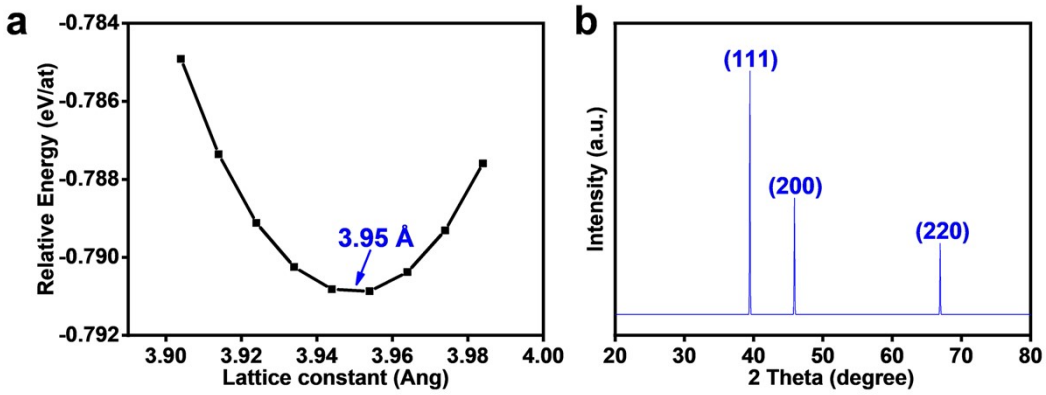

Figure S5. (a) The energy of the alloy model structure relative to (Cu+Ag) as function of lattice parameter to determine the relaxed CuAg alloy structure. (b) Simulated powder XRD profile of CuAg alloy with lattice constant of 0.395 nm.

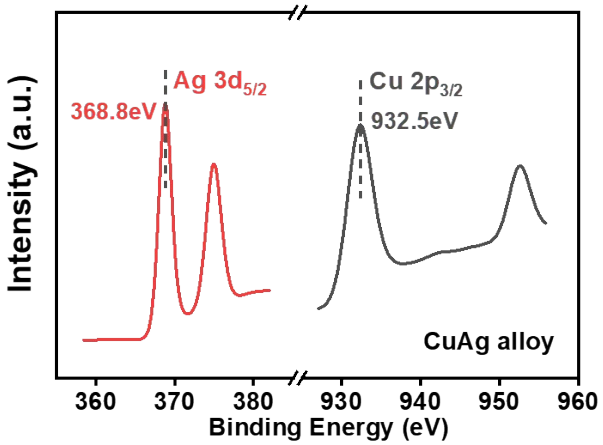

Figure S6. XPS spectra of CuAg alloy.

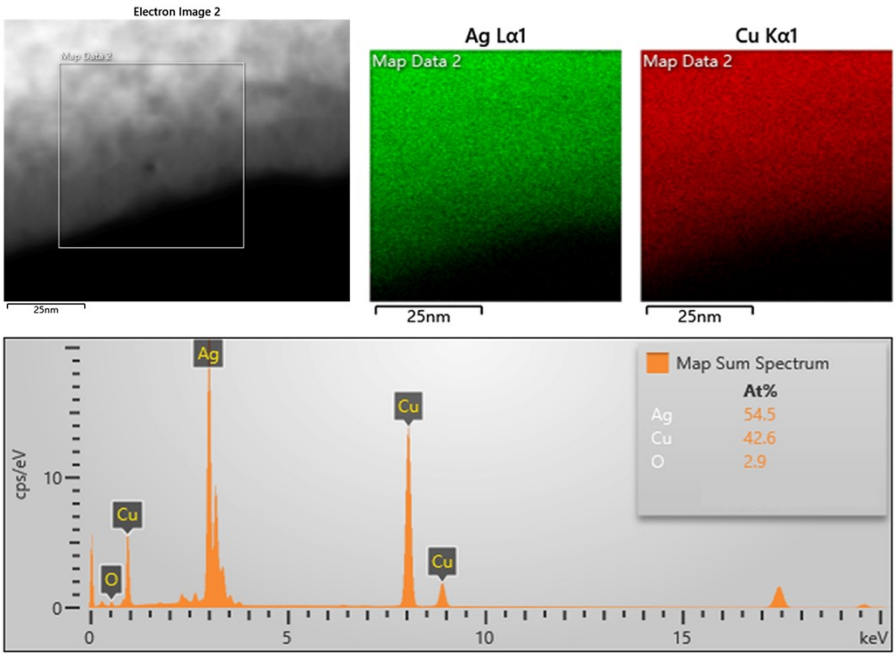

Figure S7. TEM-EDS mapping spectra of CuAg alloy.

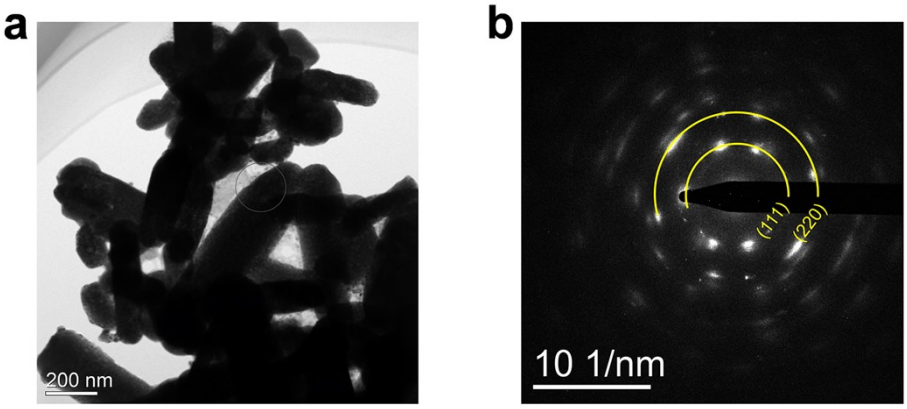

Figure S8. Selected area electron diffraction (SAED) pattern of CuAg alloy nanorods. Some diffraction spots in (b) are semi-circled in yellow using relaxed lattice parameter of model structure of solid-solution CuAg in Figure S4.

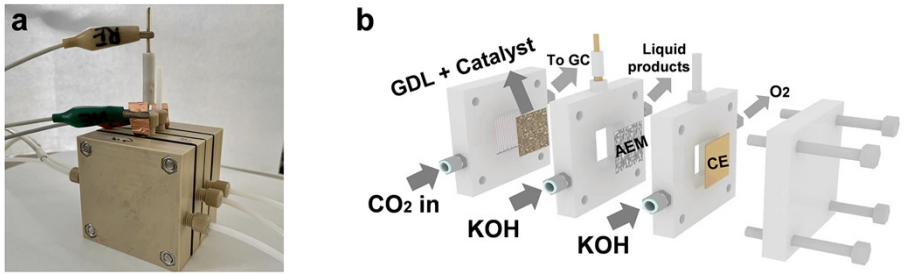

Figure S9. (a) Photograph of the flow cell used for electrocatalytic CO_2 reduction. (b) Isometric view of the exploded three-chamber GDE showing the various components.

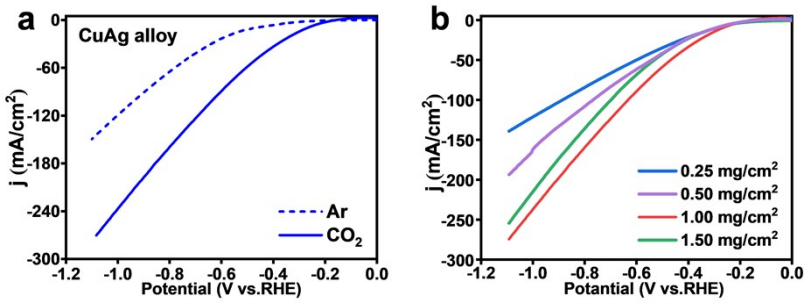

Figure S10. (a) LSV curves of CuAg alloy measured in Ar and CO_2 with a flow cell. (b) LSV curves of CuAg alloy with different loading for ECR.

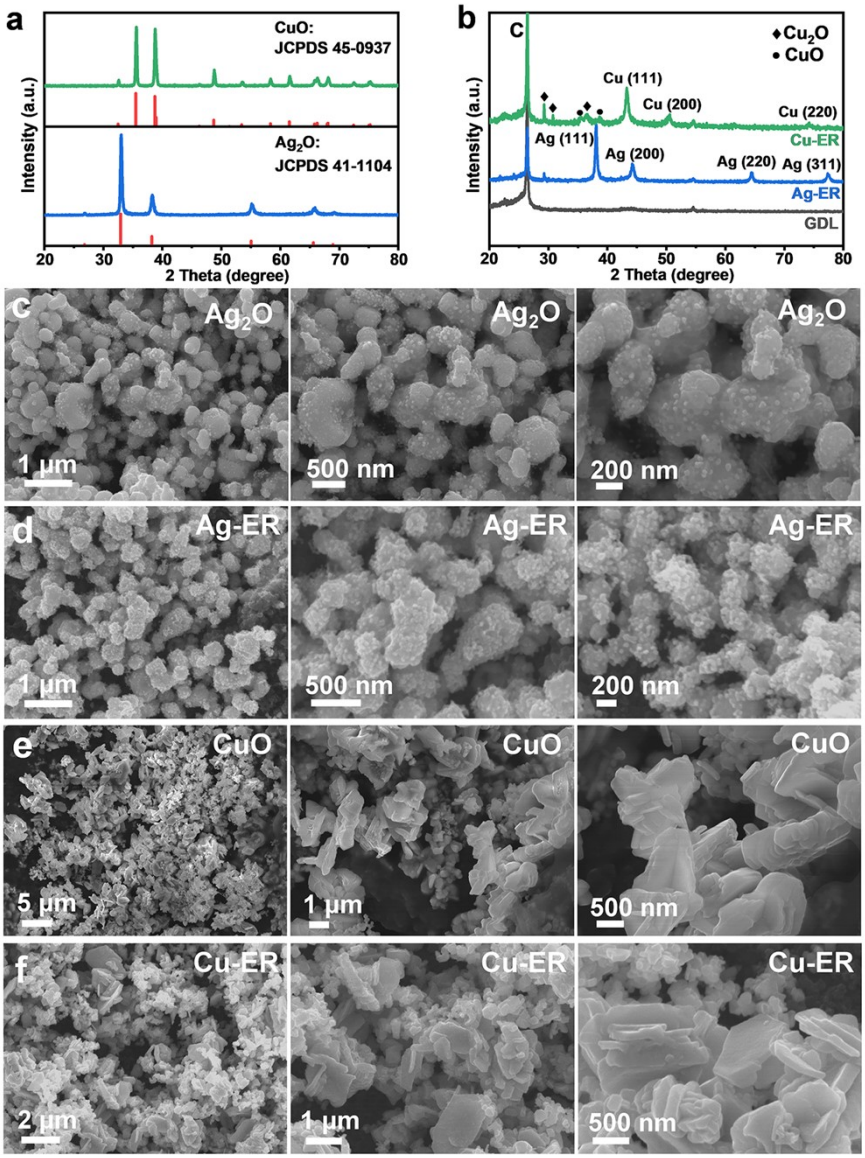

Figure S11. Characterization of reference CuO and Ag_2O materials. XRD profile before (a) and after (b) electrochemical reduction (ER) using the same procedure that solid-solution CuAg alloy is synthesized from $Cu_2Ag_2O_3$. For both CuO and Ag_2O, oxide residuals are found, which can be attributed to rapid formation of compact metal layer on the oxide surface and in turn incomplete reduction. SEM images at different magnification for oxides before (c, e) and after electrochemical reduction (d, f).

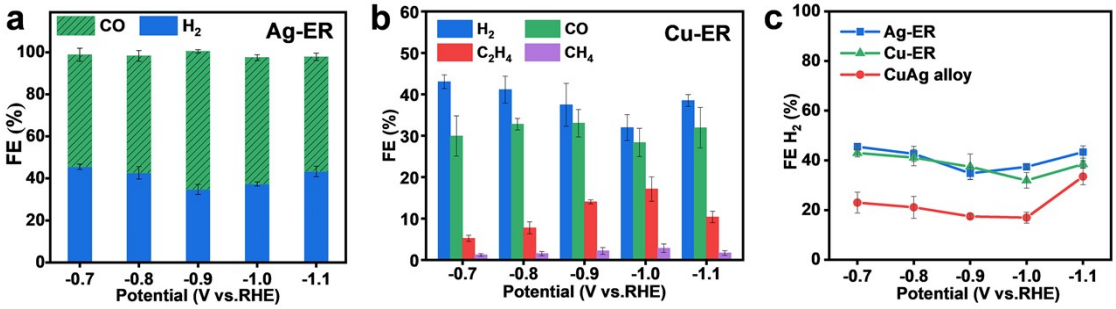

Figure S12. Faradaic efficiencies of gas products on different ECR catalysts. (a) Electro-reduced Ag_2O (Ag-ER). (b) Electro-reduced CuO (Cu-ER). (c) Comparison of H_2 FE of the three samples showing that the solid-solution CuAg alloy has the lowest selectivity for H_2 at all applied potentials.

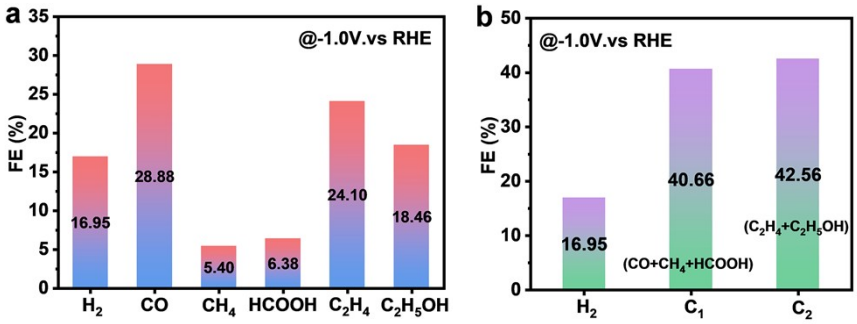

Figure S13. Faradaic efficiencies of products of CuAg alloy in ECR at -1.0 V (RHE).

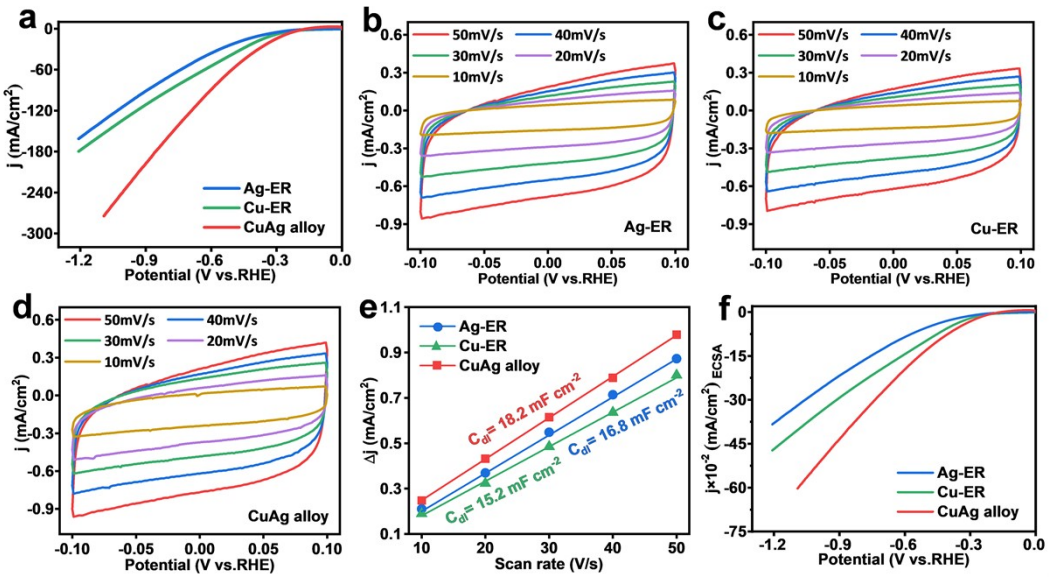

Figure S14. (a) LSV curves measured in a flow cell of three metal ECR catalyst prepared by electro-reduction by applying a -5.0 V large overpotential starting from $Cu_2Ag_2O_3$, CuO, and Ag_2O. (b-e) Determination of the electrochemical surface area (ECSA) by measuring the double-layer capacitance from CVs at different scan rates. (f) ECSA normalized LSV curves of the three catalysts.

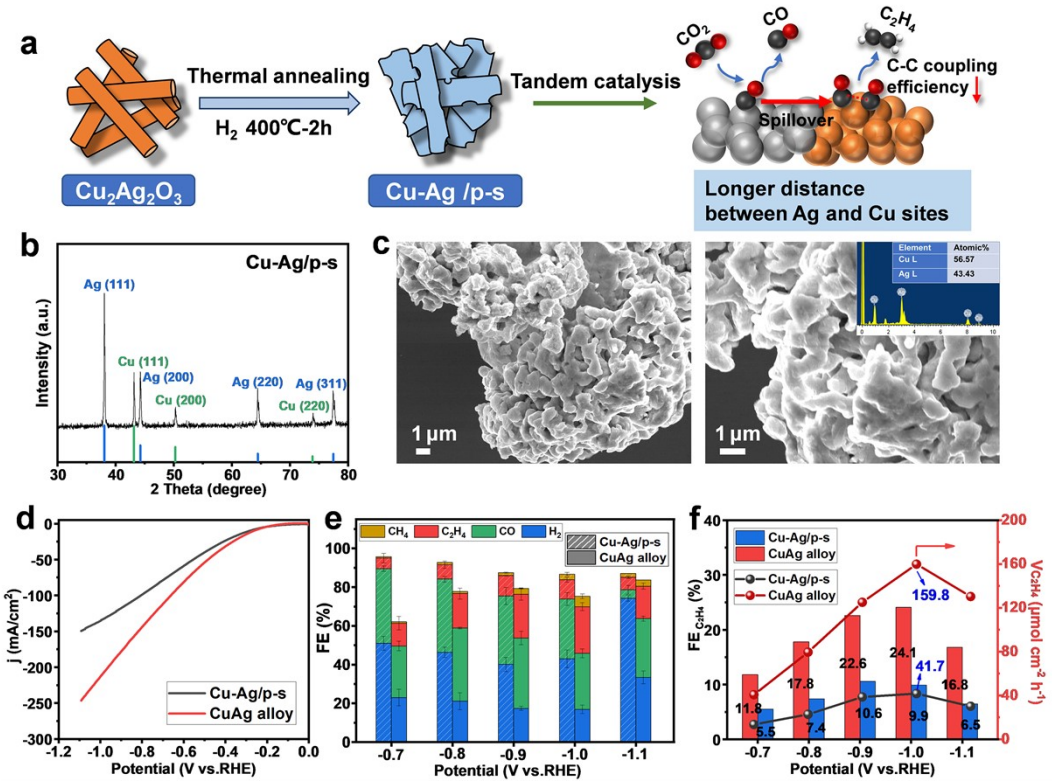

Figure S15. (a) Schematic diagram of preparation of phase-separated Cu-Ag alloy from $Cu_2Ag_2O_3$ by thermal annealing in H_2 flow (denoted as Cu-Ag/p-s). (b) XRD profile of Cu-Ag/p-s. (c) SEM images of Cu-Ag/p-s and corresponding EDS pattern. (d) LSV curves of phase-separated Cu-Ag/p-s. (e) Faradaic efficiencies of gas products of the two alloys at various potentials. (f) Faradaic efficiencies and formation rates of C_2H_4.

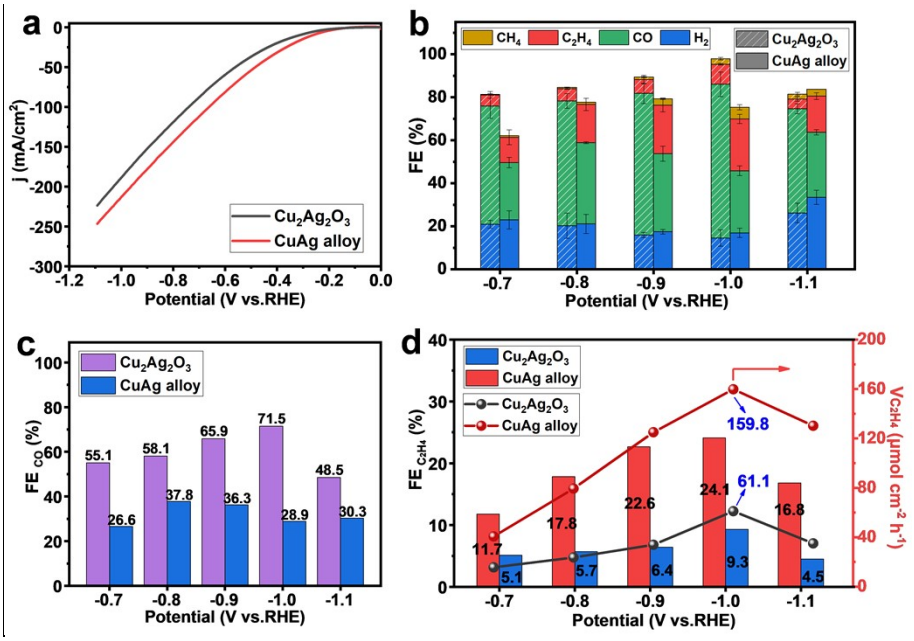

Figure S16. Comparative study of $Cu_2Ag_2O_3$ and CuAg alloy catalysts for ECR. (a) LSV curves. (b) Faradaic efficiencies (FE) of gas products at different applied potentials. (c) CO FE at various potentials. (d) FEs and formation rates of C_2H_4 at various potentials.

Table S1. Faradaic efficiency of products for three samples at -1.0 V (RHE) in ECR.

Materials	H_2 (FE/%)	CO (FE/%)	CH_4 (FE/%)	C_2H_4 (FE/%)	HCOOH (FE/%)	C_2H_5OH (FE/%)	C_1 production total (FE/%)	C_2 production total (FE/%)
Ag	37.39	60.07	-	-	-	-	60.07	-
Cu	31.95	28.36	2.85	**17.12**	11.13	6.22	42.34	**23.34**
CuAg	16.95	28.88	5.40	**24.10**	6.38	18.46	40.66	**42.56**